CHAPTER III

Effect of Magnetic Field on Steady Boundary Layer Slip Flow along with Heat and Mass Transfer over a Flat Porous Plate Embedded in a Porous Medium

3.1. Introduction

The heat and mass transfer of viscous incompressible fluid flow over a porous plate in the presence of magnetic field has tremendous applications in many engineering fields such as heat exchanger devices, petroleum reservoirs, chemical catalytic reactors and processes, geothermal and geophysical engineering, aerodynamic engineering and others.

The effect of magnetic field on heat and mass transfer under various physical conditions was investigated by several authors. Hydromagnetic mixed convective heat and mass transfer over a vertical plate with a convective surface boundary condition was studied by Aziz (2009). Freidoonimehr, Rashidi and Jailpour (2015) studied the heat and mass transfer in an incompressible steady laminar MHD flow using the combination of differential transform method and Padé approximant. The effect of magnetic field on free convective heat transfer was studied by Sparrow and Cess (1961). It was observed that the free convective heat transfer to liquid metals was affected significantly by magnetic field, but other fluids experienced negligible effects.

Andersson (2002) studied the slip effects on boundary layer stagnation-point flow and heat transfer towards a shrinking sheet and later it was extended by Santosh Chaudhary and Pradeep Kumar (2013) for viscous, incompressible, electrically conducting fluid near a stagnation point past a shrinking sheet with slip in the presence of a magnetic field. Anjalidevi and Kandaswamy (2000) explored the effects of magnetic field on heat and mass transfer flow along a semi-infinite horizontal plate. Thermal radiation and non-uniform magnetic field was considered by Mohammad Mehdi Rashidi *et al.* (2014) who employed the homotopy analysis method. Pal and Talukdar (2010) studied an unsteady MHD convective heat and mass transfer in the presence of thermal radiation and chemical reaction using perturbation method. Gangadhar *et al.* (2012) studied the similarity solution of hydromagnetic heat and

mass transfer over a vertical plate with convective surface boundary condition and chemical reaction.

The effect of temperature-dependent viscosity on free convective flow past a vertical porous plate was studied by Makinde (2010) in the presence of a magnetic field without heat source and with heat source. Asim Aziz *et al.* (2014) studied the steady boundary layer slip flow along heat and mass transfer in porous medium.

The absence of magnetic field in Asim Aziz *et al.* (2014) motivated us to take up the present work wherein we study, the steady boundary layer slip flow along with heat and mass transfer over a flat porous plate embedded in a porous medium in the presence of a varying magnetic field. In order to examine the accuracy of our result, the effect of various parameters on velocity, temperature and concentration are calculated and plotted. The results obtained are validated for vanishing magnetic field which is same as the result obtained by Asim Aziz *et al.* (2014).

3.2. Flow Description and Governing Equations

We consider a steady two dimensional laminar flow of a viscous incompressible electrically conducting fluid with heat and mass transfer over a porous flat plate in the presence of transverse magnetic field embedded in a porous medium. The x-axis is taken along the plate and the y-axis is taken normal to the plate. In order to simplify the model, all body forces are neglected and we assume that the fluid flow is stable.

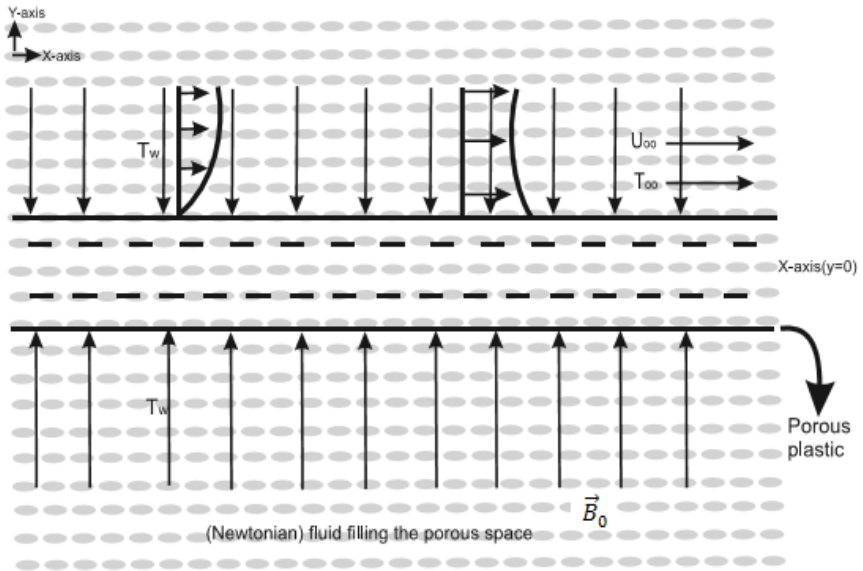

Fig 3.1 Schematic diagram of the problem

In the present work, the following assumptions are made:

- Flow of a Newtonian fluid is considered, which is steady, viscous, laminar, incompressible and electrically conducting.
- All fluid properties are assumed to be independent of temperature.
- Magnetic field is applied perpendicular to the plane of the plates.
- Body forces in the momentum equation are neglected.
- Viscous dissipation effect and heat source are not considered in the heat conduction equation.

Under these assumptions, the governing equations for the continuity, momentum and energy are taken in the following form.

$$\frac{\partial u}{\partial x}+\frac{\partial v}{\partial y}=0 \tag{3.1}$$

$$u\frac{\partial u}{\partial x}+v\frac{\partial u}{\partial y}=\gamma\frac{\partial^2 u}{\partial y^2}-\frac{\gamma}{k}(u-U_\infty)+\frac{\sigma B_0^2}{\rho}(U_\infty-u) \tag{3.2}$$

$$u\frac{\partial T}{\partial x}+v\frac{\partial T}{\partial y}=\frac{\kappa}{\rho C_p}\frac{\partial^2 T}{\partial y^2} \tag{3.3}$$

$$u\frac{\partial C}{\partial x}+v\frac{\partial C}{\partial y}=D_M\frac{\partial^2 C}{\partial y^2}+D_T\frac{\partial^2 T}{\partial y^2} \tag{3.4}$$

In the above system of equations, u and v represent velocity components in x and y directions respectively. T, C, μ, ρ, σ and $\gamma=(\mu/\rho)$ represent respectively the temperature, mass concentration, coefficient of viscosity, density, electrical conductivity and kinematic viscosity of the fluid. The constant parameters in the system: $k, C_p, \kappa,$ D_M and D_T respectively denote the permeability of porous material, specific heat at constant pressure, thermal conductivity of the fluid, molecular diffusivity and thermal diffusivity. $\vec{B}(x)$ is the magnetic field in the y-direction and is given by $\vec{B}(x)=B_0/(x)^{1/2}.\hat{j}$.

The appropriate boundary conditions for velocity, temperature and mass concentration are given by,

$$u=L_1\left(\frac{\partial u}{\partial y}\right),\ v=v_w \text{ at y=0};\ u\to U_\infty \text{ as } y\to\infty, \tag{3.5}$$

$$T=T_w+D_1\left(\frac{\partial T}{\partial y}\right) \text{ at } y=0;\ T\to T_\infty \text{ as } y\to\infty\ , \tag{3.6}$$

$$C=C_w+N_1\left(\frac{\partial C}{\partial y}\right) \text{ at } y=0;\ C\to C_\infty \text{ as } y\to\infty\ , \tag{3.7}$$

In equations (3.5)-(3.7) $L_1=L(Re_x)^{1/2}$ is the velocity slip factor, $D_1=D(Re_x)^{1/2}$ is the thermal slip factor and $N_1=N(Re_x)^{1/2}$ is the mass slip factor. Here L, D and N are the initial values of velocity, thermal and mass slip factors respectively

and L, D and N all three have dimensions of length. Moreover, U_∞, T_∞ and C_∞ denote free stream velocity, free stream temperature, and free stream mass concentration respectively. In these equations T_w and C_w represent the temperature and mass concentration of the plate respectively. The velocity v_w defines suction or blowing through the porous plate and is written as $v_w = v_0/\sqrt{x}$. In this relation v_0 is constant linked with suction if $v_0 < 0$ and blowing when $v_0 > 0$.

We introduce the stream function $\psi(x, y)$ as

$$u = \frac{\partial \psi}{\partial y}\ ,\ v = -\frac{\partial \psi}{\partial x} \tag{3.8}$$

3.3. Solution of the Problem

In this work, similarity technique is used to solve the system of equations (3.1)-(3.4) along with the boundary conditions (3.5)-(3.7). The similarity transformations are,

$$\psi = \sqrt{U_\infty \gamma x} f(\eta),\ \theta(\eta) = \frac{T - T_\infty}{T_w - T_\infty},\ \phi(\eta) = \frac{C(x) - C_\infty}{(C_w - C_\infty)x}, \tag{3.9}$$

where η is the similarity variable defined as $\eta = \sqrt{Re_x}(y/x)$.

Introducing the above transformations in equations (3.1)-(3.4), we obtain the system of ordinary differential equations,

$$f''' + \frac{1}{2} f f'' - k^*(f' - 1) - M(f' - 1) = 0, \tag{3.10}$$

$$\theta'' + \frac{1}{2} Pr f \theta' = 0, \tag{3.11}$$

$$\phi'' - Scf'\phi + \frac{1}{2} Scf\phi' + ScSr\theta'' = 0 \tag{3.12}$$

In equation (3.10), $k^* = 1/Da_x Re_x$ represents the permeability of porous medium and $Da_x = k/a^2 = k_0/x$ is the local Darcy number. Here k_0 is the constant and $M = \frac{\sigma B_0^2 x}{\rho U_\infty}$ is the magnetic parameter. In equation (3.11) $Pr = \mu C_p/\kappa$ is the Prandtl number. Finally in equation (3.12), $Sc = \frac{\gamma}{D_m}$ is the Schmidt number and $Sr = \frac{(T_w - T_\infty) D_T}{(C_w - C_\infty) x \gamma}$ is the Soret number.

The boundary conditions (3.5)-(3.7) transform to the following form,

$$f(\eta) = S,\quad f'(\eta) = \delta f''(\eta) \text{ at } \eta = 0; \qquad f'(\eta) \to 1 \text{ as } \eta \to \infty \tag{3.13}$$

$$\theta(\eta) = 1 + \beta\theta'(\eta) \text{ at } \eta = 0; \quad \theta(\eta) \to 0 \text{ as } \eta \to \infty \tag{3.14}$$

$$\phi = 1 + \varsigma\phi' \text{ at } \eta = 0; \quad \phi \to 0 \text{ as } \eta \to \infty \tag{3.15}$$

where $S = (-2v_w/U_\infty)(Re_x)^{1/2} = -2v_0/(U_\infty \gamma)^{1/2}$, $S > 0$ (i.e.$v_0 < 0$) corresponds to suction and $S < 0$ (i.e.$v_0 > 0$) corresponds to blowing, $\delta = LU_\infty/\gamma$ is the velocity

slip parameter, $\beta = DU_\infty/\gamma$ is the thermal slip parameter and $\varsigma = NU_\infty/\gamma$ is a mass slip parameter.

The non-linear coupled ordinary differential equations (3.10)-(3.12) subject to boundary conditions (3.13)-(3.15) are reduced to a system of first order ordinary differential equations as follows,

$$f' = w,\ \ w' = v,\ v' = -0.5fv + k^*(w-1) + M(w-1), \tag{3.16}$$

$$\theta' = z,\quad z' = -0.5Prfz, \tag{3.17}$$

$$\phi' = e,\ e' = Scwb - 0.5Scfe - ScSrz' \tag{3.18}$$

and boundary conditions become,

$$x(0) = S,\ w(0) = \delta v(0),\quad y(0) = 1 + \beta z(0),\ \ b(0) = 1 + \varsigma e(0) \text{ at } \eta = 0 \tag{3.19}$$

$$w(0) \to 1, y(0) \to 0, b(0) \to 0 \text{ as } \eta \to \infty \tag{3.20}$$

We have solved the equations (3.16)-(3.18) with boundary conditions (3.19) and (3.20) using shooting method.

The major physical quantities - the skin-friction coefficient C_f, the local Nusselt number Nu_x, and the local Sherwood number Sh_x are defined respectively as follows,

Skin-friction co-efficient: $C_f = \frac{\tau_w}{\rho U_w^2 x}$

Local Nusselt number: $Nu_x = \frac{xq_w}{k(T_w - T_\infty)}$

Local Sherwood number: $Sh_x = \frac{xq_m}{D_A(C_w - C_\infty)}$

where $\tau_w$is the skin-friction, q_w is the heat flux, q_m is the mass flux at the surface respectively.

$$\tau_w = \mu\left(\frac{\partial u}{\partial y}\right)_{y=0},\ q_w = -k\left(\frac{\partial T}{\partial y}\right)_{y=0},\ q_m = -D_B\left(\frac{\partial C}{\partial y}\right)_{y=0}$$

Applying the non-dimensional transformations (3.9) we obtain,

$$f''(0) = C_f(Re_x)^{1/2},$$

$$-\theta'(0) = Nu_x(Re_x)^{-1/2},$$

$$-\phi'(0) = xSh_x(Re_x)^{-1/2}$$

where $Re_x = \frac{xU_\infty}{\gamma}$ is the local Reynolds number.

3.4. Results and Discussion

In order to get physical insight of the problem we have studied the velocity, temperature and concentration against various parameters such as magnetic parameter M, the velocity slip parameter δ, thermal slip parameter β, mass slip parameter ς,

Schmidt number Sc and Soret number Sr. The effect of flow parameters on velocity field, skin-friction, Nusselt number and Sherwood number are calculated numerically and discussed with the help of graphs.

We have shown the velocity, temperature and concentration of various values of permeability parameter k* through figures (3.2)-(3.4) for vanishing magnetic field. It can be seen from these figures increase in permeability causes an increase in velocity, decrease in temperature and concentration profiles for both slip and no-slip conditions. These results are in good agreement with Asim Aziz *et al.* (2014).

Figures (3.5)-(3.7) depict the influence of magnetic field M on the velocity, temperature and concentration profiles for both slip and no-slip conditions. We observe that the velocity $f'(\eta)$ along the plate increases when magnetic field increases. Consequently temperature $\theta(\eta)$ and concentration $\phi(\eta)$ profiles decrease when magnetic field increases for both slip and no-slip conditions.

Figures (3.8)-(3.10) show the variation in shear stress $f''(\eta)$, the rate of heat and mass transfer for several values of magnetic parameter M. We observe that the increase in magnetic parameter M causes increase in shear stress $f''(\eta)$ and decrease in the rate of heat and mass transfer.

Figures (3.11)-(3.16) explain about the effect of slip parameter δ on the velocity, temperature and concentration profiles, shear stress and the rate of heat and mass transfer. It can be inferred from these graphs that increase in velocity slip parameter δ results in the enhancement of velocity and the rate of mass transfer while, the shear stress, temperature, concentration and the rate of heat transfer decrease due to the increase of slip parameter δ.

Figures (3.17) and (3.18) represent the effect of slip parameter β on temperature and the rate of heat transfer. We can observe from these graphs that the increase in slip parameter β results in decrease in temperature and increase in rate of heat transfer.

Figures (3.19) and (3.20) show the effect of mass slip parameter ς on concentration and the rate of mass transfer. We can observe that the increase in slip parameter ς results in decrease in concentration and increase in rate of mass transfer.

Figures (3.21)-(3.23) depict that the variation in velocity, temperature and concentration profiles for different values of suction/blowing parameter S. Here, S>0 shows the suction and S<0 shows the blowing. When suction increases, i.e., S>0, fluid

velocity increases, which in turn decreases both the fluid boundary layer and the thickness of momentum boundary layer. Due to suction of the fluid particles at the porous wall, velocity profile increases. In the case of blowing S<0, the opposite trend is observed. When suction increases i.e., S>0, fluid particles come close to the porous wall, due to this temperature profile decreases, which in turn decreases the thermal boundary layer. When suction is increased i.e., S>0, the mass concentration decreases. An opposite phenomena is observed for blowing.

Figures (3.24) and (3.25) explain the effect of Schmidt number Sc and Soret number Sr on concentration profiles. These two figures illustrate that the increase in Schmidt number and Soret number causes decrease and increase in concentration profiles for both slip and no-slip conditions respectively.

Figures (3.26) and (3.27) illustrate the effect of Schmidt number Sc and Soret number Sr on the rate of mass transfer. These two figures illustrate that the increase in Schmidt number and Soret number causes decrease and increase in $\phi'(0)$ for both slip and no-slip conditions respectively.

Figure (3.28) shows skin-friction coefficient $f''(0)$ as a function of the slip parameter δ for various values of magnetic parameter M. It is clear that skin-friction decreases rapidly and approaches zero as the slip parameter δ increases.

Figures (3.29) and (3.30) show the rate of heat transfer $\theta'(0)$ as a function of the slip parameters δ and β for various values of magnetic parameter M. We can observe that increase in slip parameters δ and β causes decrease and increase in the rate of heat transfer $\theta'(0)$ respectively.

Figures (3.31)-(3.33) exhibit the rate of mass transfer $\phi'(0)$ as a function of the slip parameters δ, β, and ς for various values of magnetic parameter M. We can observe that the rate of mass transfer $\phi'(0)$ decreases, as there is increase in slip parameter δ and β and magnetic parameter M respectively. We can also observe that the rate of mass transfer $\phi'(0)$ increases, with increase in slip parameter ς.

3.5. Conclusion

The effect of MHD convective boundary layer flow along with heat and mass transfer over a porous plate embedded in a porous medium has been investigated. The similarity transformations are used to transform the governing partial differential equations (PDEs) into a system of nonlinear ordinary differential equations (ODEs). The resulting system of ODEs is then reduced to a system of first order differential

equations which are solved by shooting procedure using fourth order Runge-Kutta method. Effect of various non-dimensional parameters on the fluid flow, heat and mass transfer characteristics are examined.

The following conclusions are drawn from the present study:

- Skin-friction decreases rapidly and approaches zero as the velocity slip parameter δ increases.
- The rate of heat transfer $\theta'(0)$ decreases, with increase in the velocity slip parameter δ and magnetic field M. Rate of heat transfer $\theta'(0)$ increases, with increase in the thermal slip parameter β.
- The rate of mass transfer $\phi'(0)$ decreases, as increase in slip parameters δ, β and magnetic parameter M and is also observed that the rate of mass transfer $\phi'(0)$ increases, with increase in slip parameter ς.

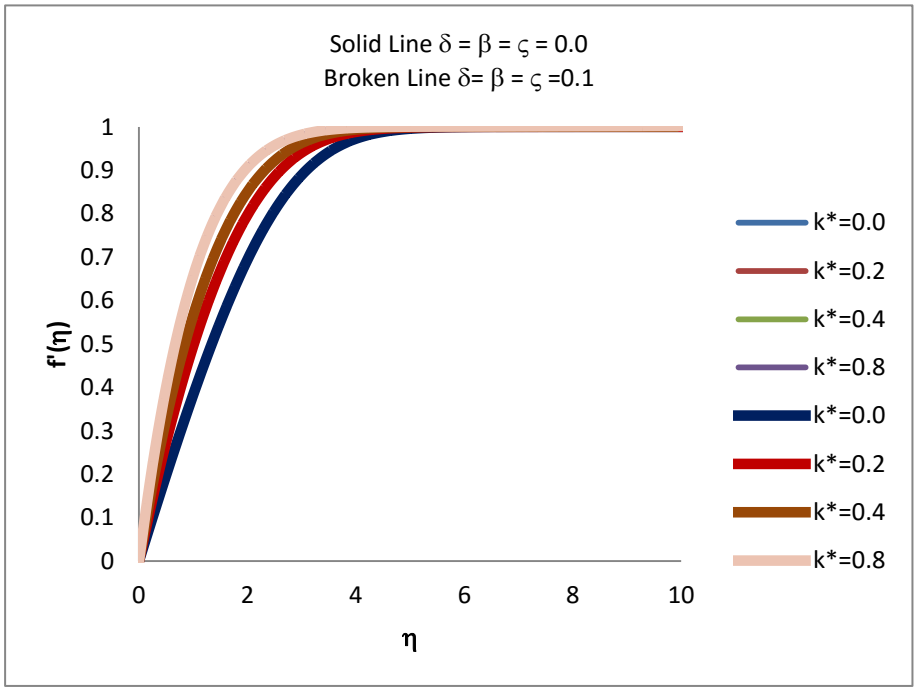

Fig 3.2 Velocity $f'(\eta)$ for various values of k with the slip and no-slip boundary conditions; S=0.2; M=0.0*

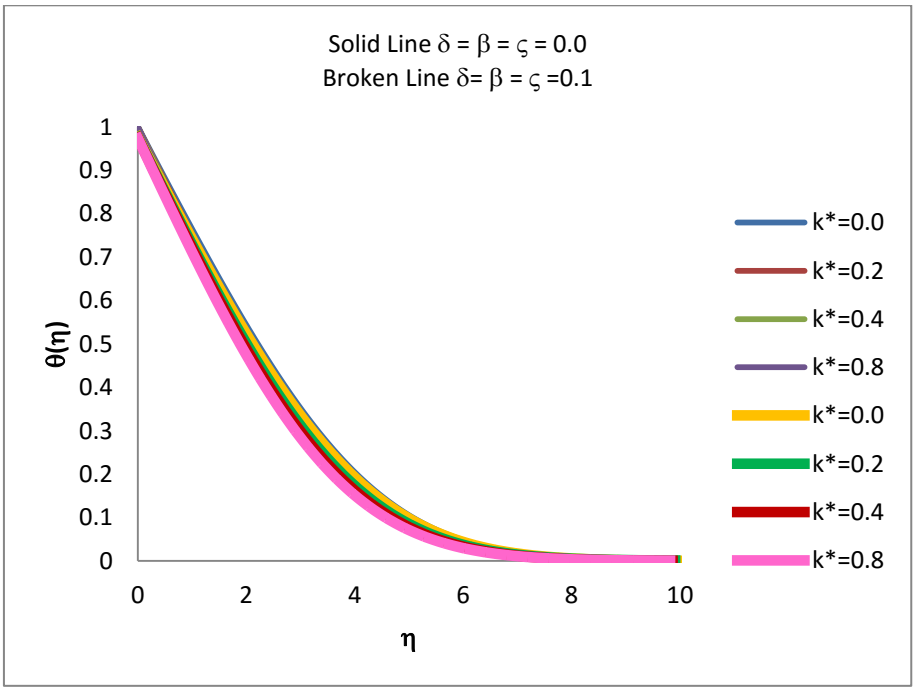

Fig 3.3 Temperature $\theta(\eta)$ for various values of k with the slip and no-slip boundary conditions; S=0.2; M=0.0*

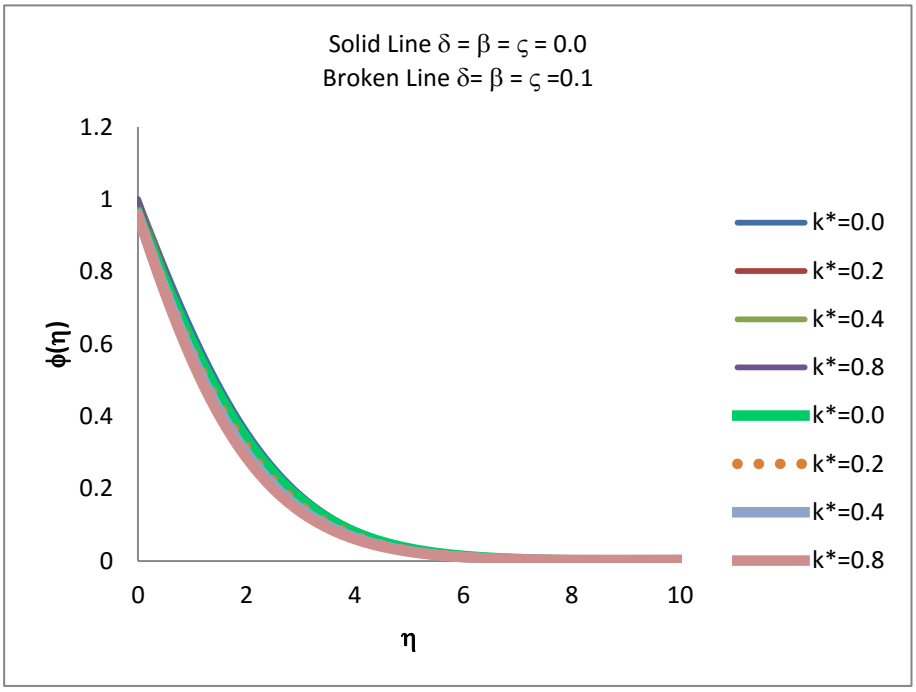

Fig 3.4 Concentration $\phi(\eta)$ for various values of k with the slip and no-slip boundary conditions; S=0.2, M=0.0.*

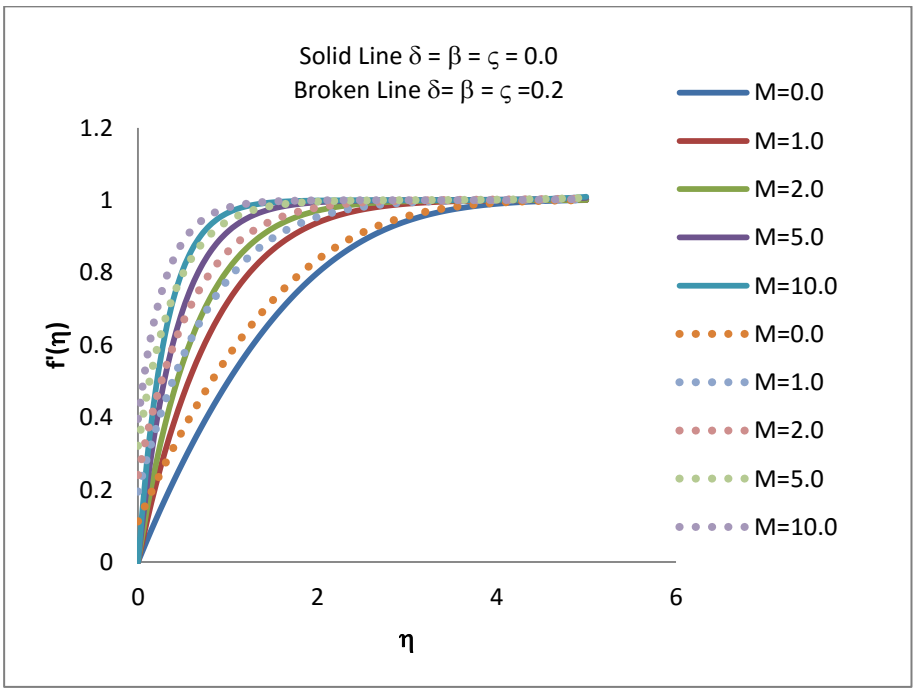

Fig 3.5 Velocity $f'(\eta)$ for various values of M with the slip and no-slip boundary conditions; Pr=7.0; S=0.2; Sc=0.3; Sr=0.3; k=0.2.*

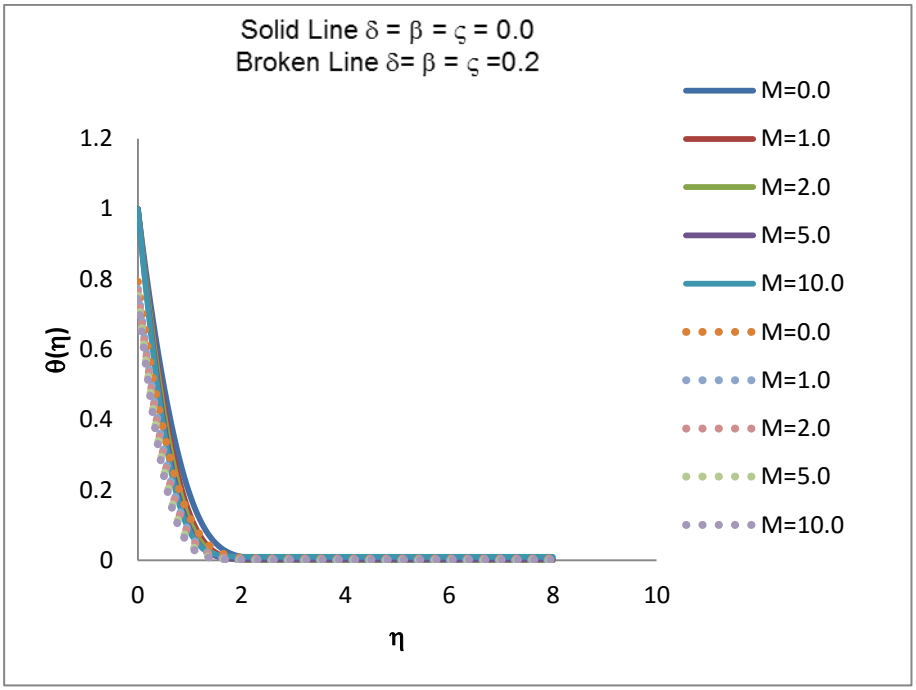

Fig 3.6 Temperature $\theta(\eta)$ for various values of M with the slip and no-slip boundary conditions; Pr=7.0; S=0.2; Sc=0.3; Sr=0.3; k=0.2*

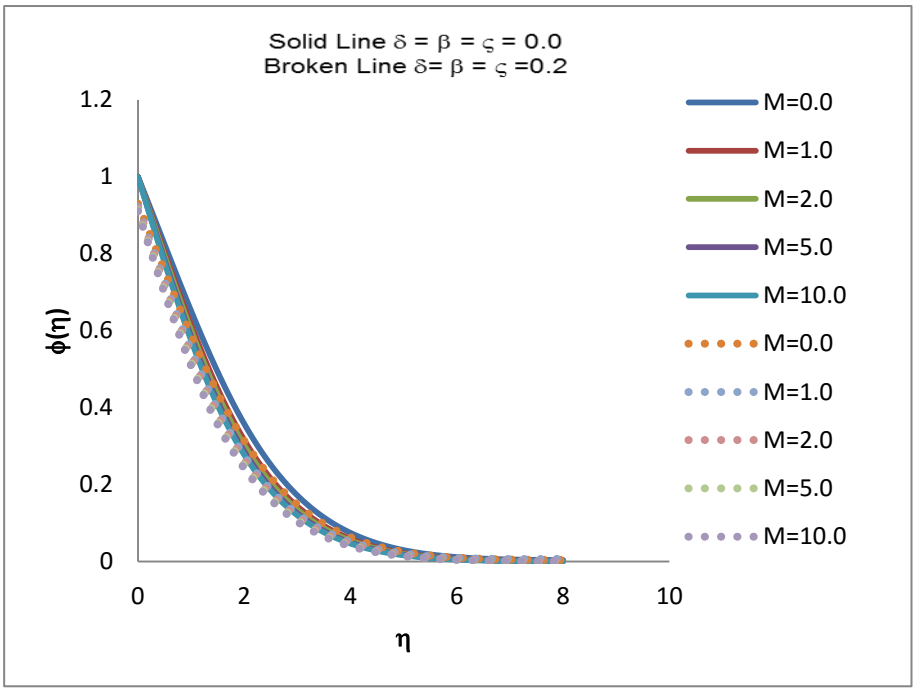

Fig 3.7 Concentration $\phi(\eta)$ for various values of M with the slip and no-slip boundary conditions; Pr = 7.0; S = 0.2; Sc = 0.3; Sr = 0.3; k = 0.2*

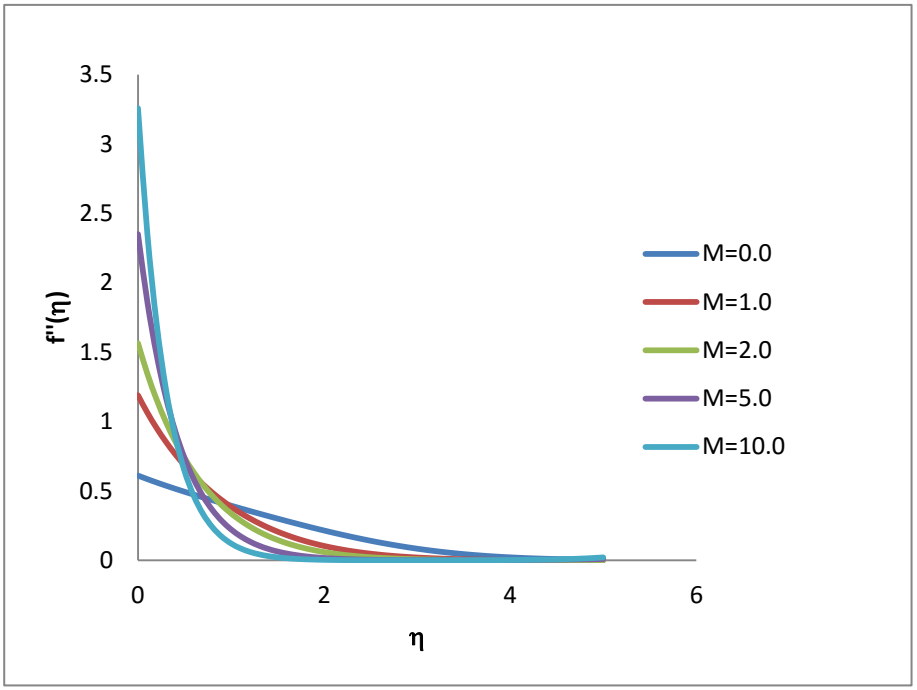

Fig 3.8 Shear stress profiles $f''(\eta)$ for various values of magnetic field M; Pr = 7.0; S = 0.2; Sc = 0.3; Sr = 0.3; k = 0.2; $\delta = \beta = \varsigma = 0.0$*

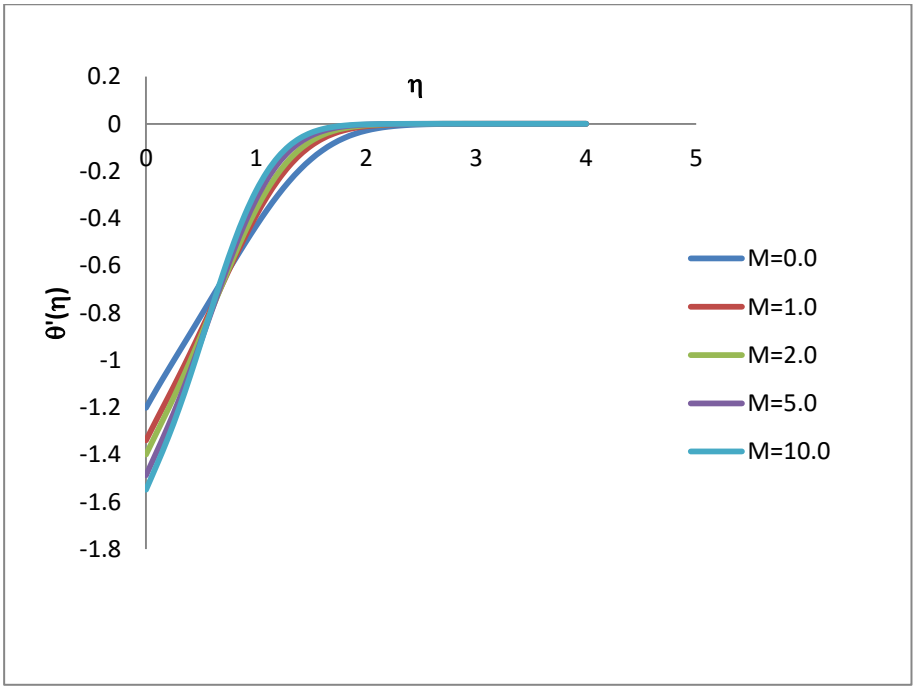

Fig 3.9 Rate of heat transfer $\theta'(\eta)$ for various values of magnetic field M; Pr = 7.0; S = 0.2; Sc = 0.3; Sr = 0.3; k = 0.2; $\delta = \beta = \varsigma = 0.0$*

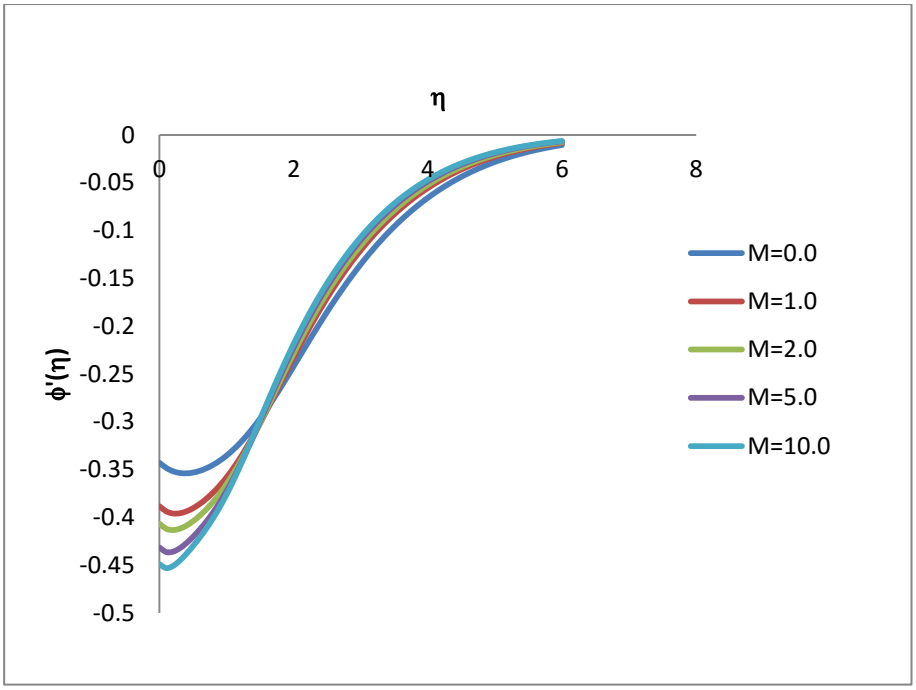

Fig 3.10 Rate of mass transfer $\phi'(\eta)$ for various values of magnetic field M; Pr = 7.0; Sc = 0.3; Sr = 0.3; S = 0.2; k = 0.2; $\delta = \beta = \varsigma = 0.0$*

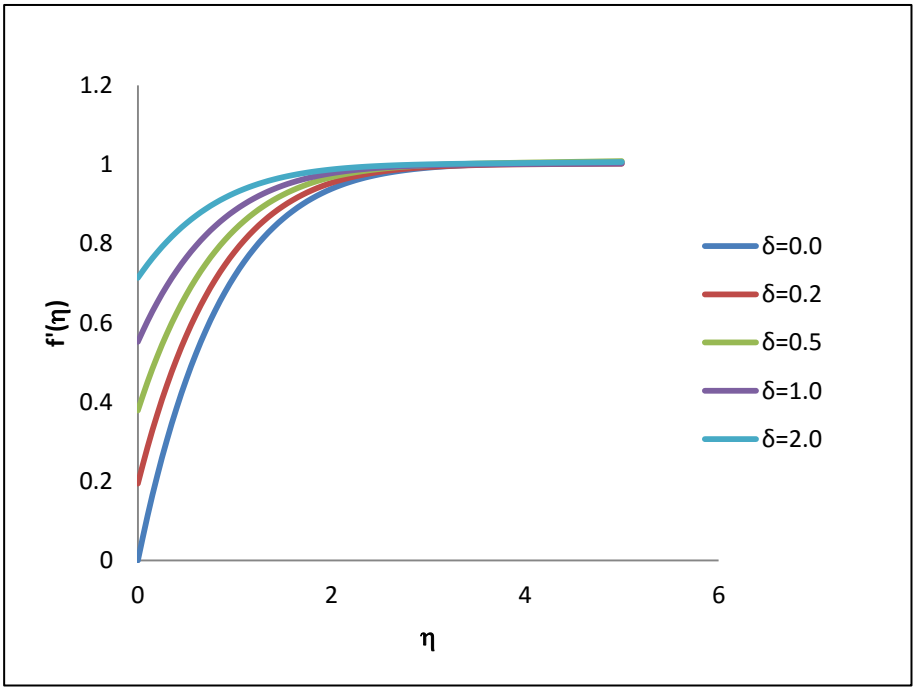

Fig 3.11 Velocity $f'(\eta)$ for various values of slip parameter δ; Pr = 7.0; Sc = 0.3; Sr = 0.3; S = 0.2; k = 0.2; M = 1.0; $\beta = 0.2$; $\varsigma = 0.2$*

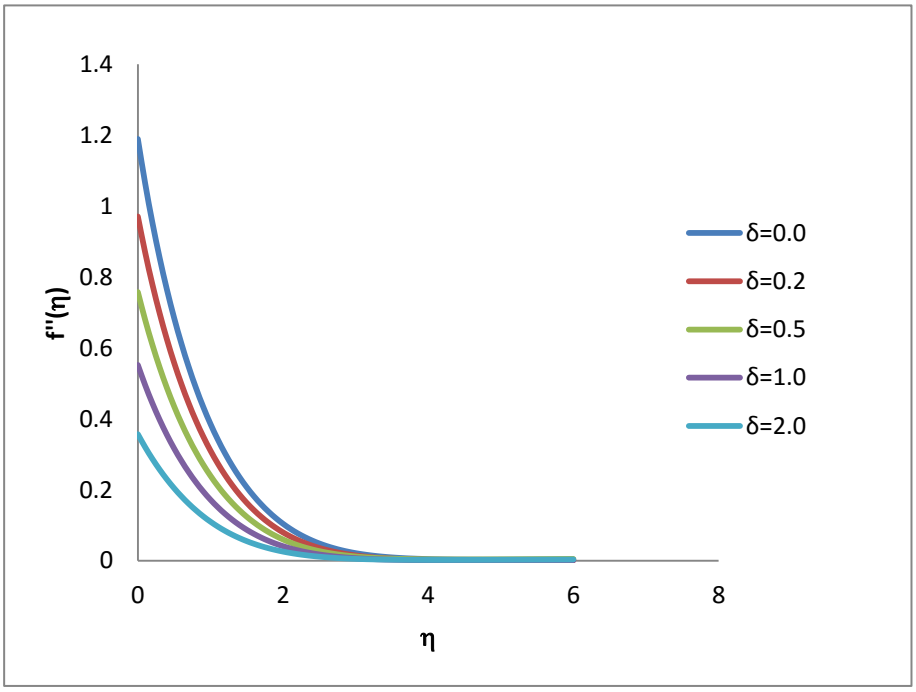

Fig 3.12 Shear stress $f''(\eta)$ for various values of slip parameter δ; Pr = 7.0; Sc = 0.3; Sr = 0.3; S = 0.2; k = 0.2 M = 1.0; β =0.2; ς = 0.2*

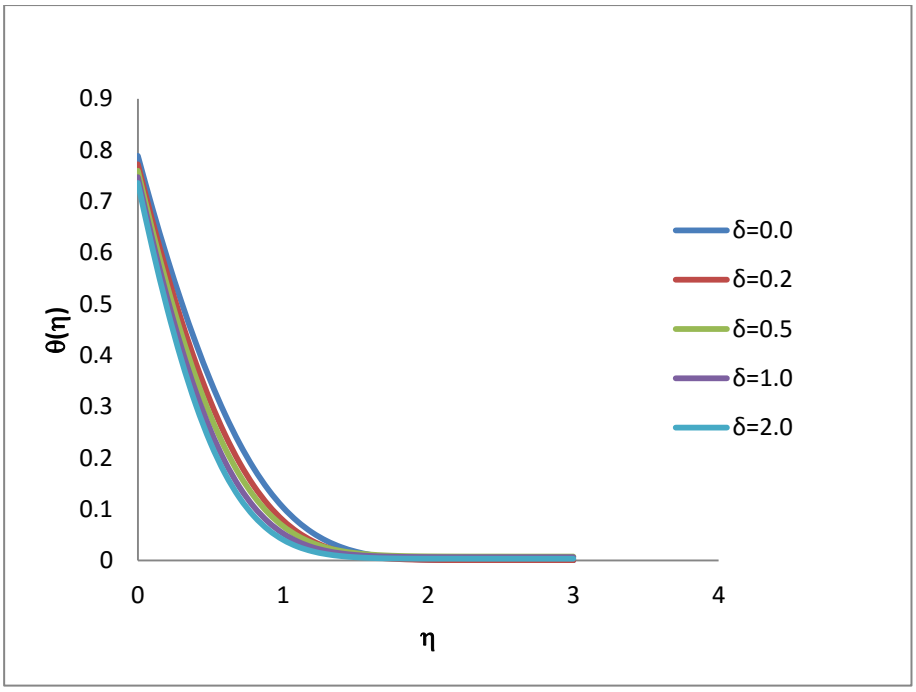

Fig 3.13 Temperature $\theta(\eta)$ for various values of slip parameter δ; Pr = 7.0; Sc = 0.3; Sr = 0.3; S = 0.2; k = 0.2; M = 1.0; β = 0.2; ς = 0.2*

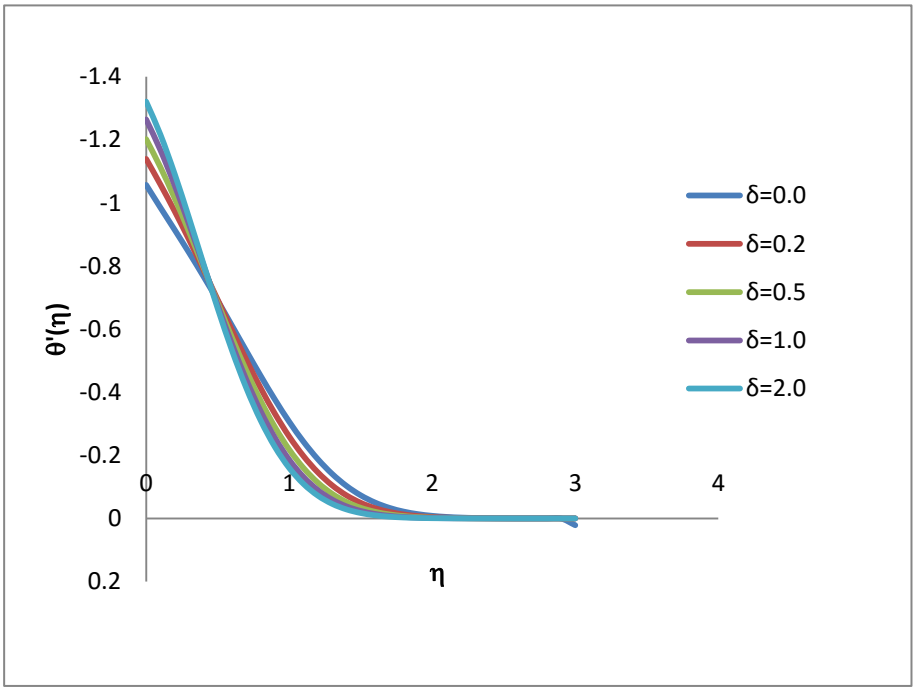

Fig 3.14 Rate of heat transfer $\theta'(\eta)$ for various values of slip parameter δ; Pr = 7.0; Sc = 0.3; Sr = 0.3; S = 0.2; k = 0.2; M = 1.0; β = 0.2; ς = 0.2*

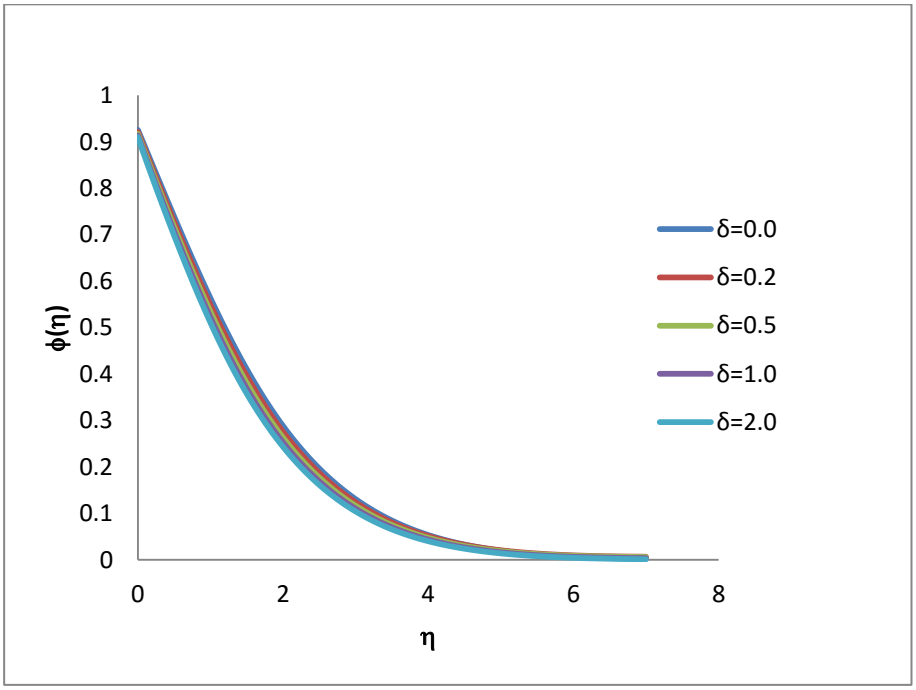

Fig 3.15 Concentration $\phi(\eta)$ for various values of slip parameter δ; Pr = 7.0; Sc = 0.3; Sr = 0.3; S = 0.2; k = 0.2; M = 1.0; β = 0.2; ς = 0.2*

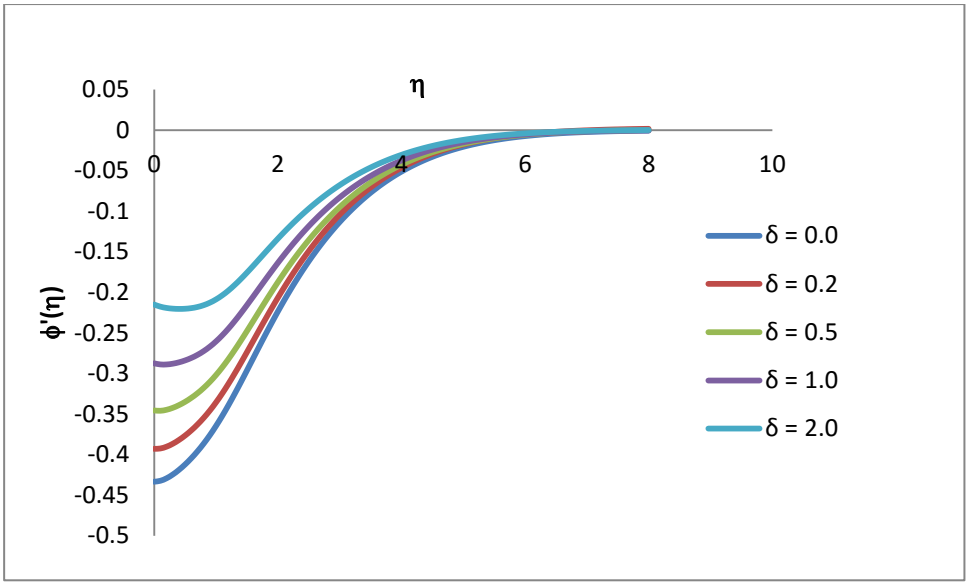

Fig 3.16 Rate of mass transfer $\phi'(\eta)$ for various values of slip parameter δ; Pr = 7.0; Sc = 0.3; Sr = 0.3; S = 0.2; k = 0.2; M = 1.0; β = 0.2; ς = 0.2*

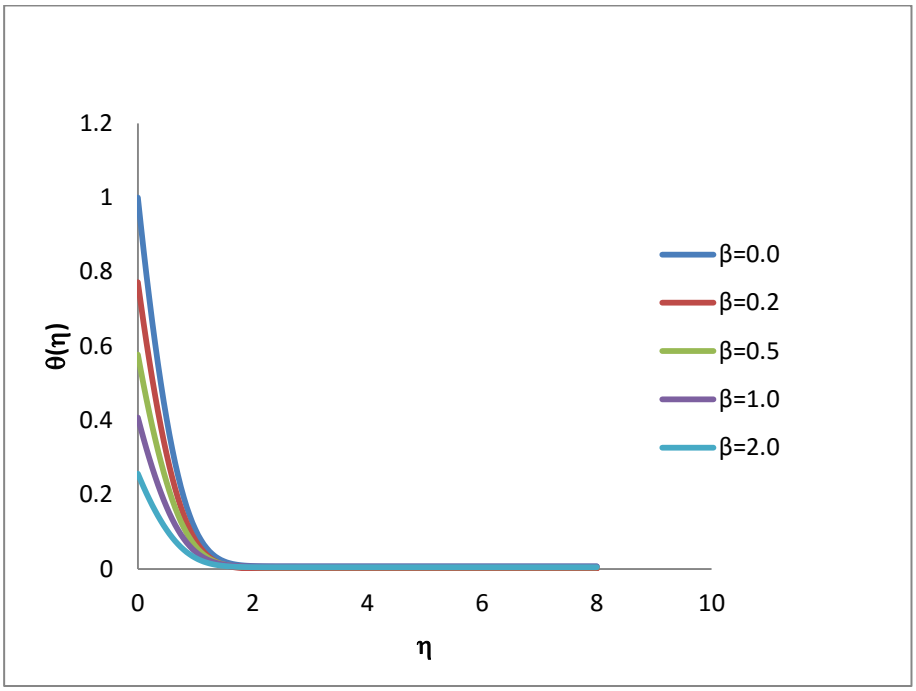

Fig 3.17 Temperature $\theta(\eta)$ for various values of slip parameter β; Pr = 7.0; Sc = 0.3; Sr = 0.3; S = 0.2; k = 0.2; M = 1.0; ς = 0.2; δ = 0.2*

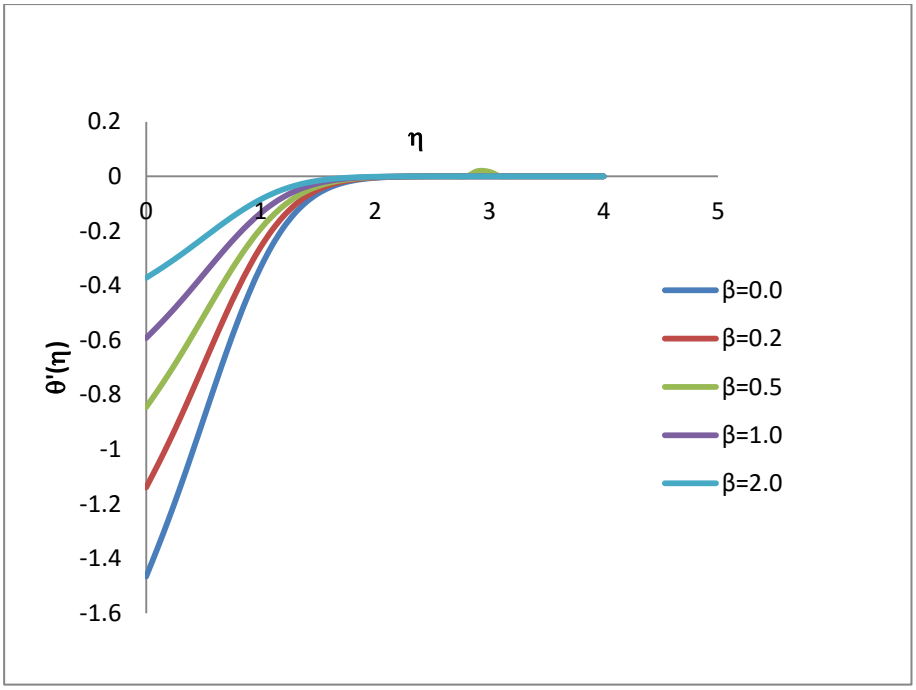

Fig 3.18 Rate of heat transfer $\theta'(\eta)$ for various values of slip parameter β; Pr = 7.0; Sc = 0.3; Sr = 0.3; S = 0.2; k = 0.2; M = 1.0; ς = 0.2; δ = 0.2*

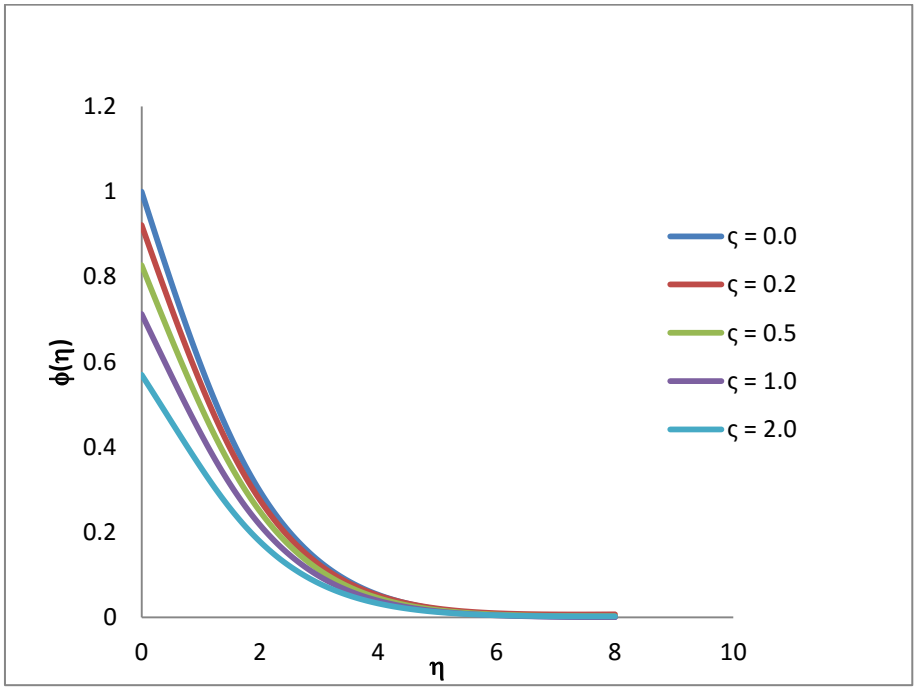

Fig 3.19 Concentration $\phi(\eta)$ for various values of slip parameter ς; Pr = 7.0; Sc = 0.3; Sr = 0.3; S = 0.2; k = 0.2; M =1.0; δ = 0.2; β = 0.2*

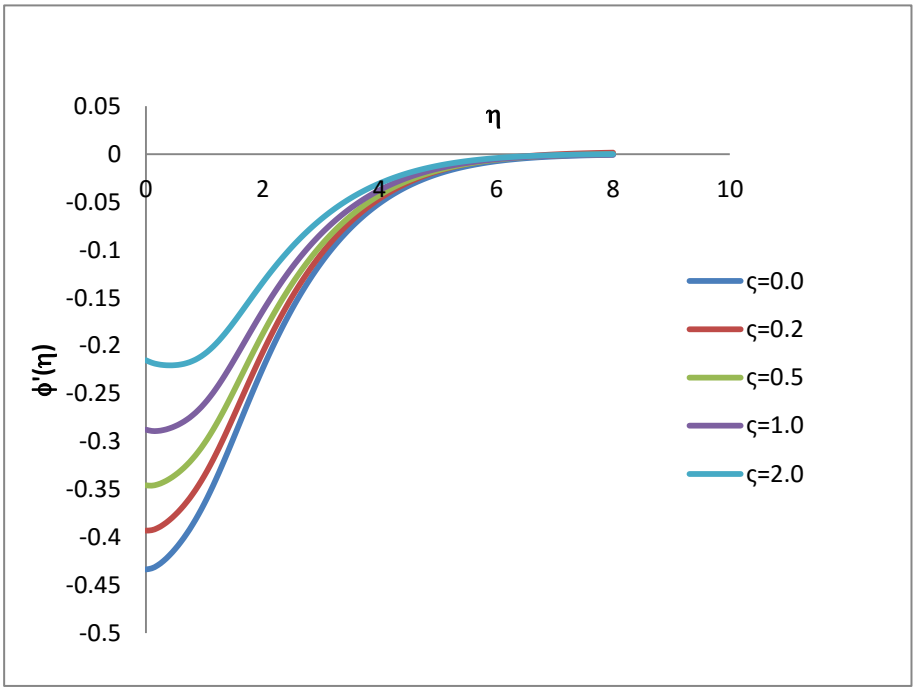

Fig 3.20 Rate of mass transfer $\phi'(\eta)$ for various values of slip parameter ς; Pr = 7.0; Sc = 0.3; Sr = 0.3; S = 0.2; k = 0.2; M = 1.0; δ = 0.2; β = 0.2*

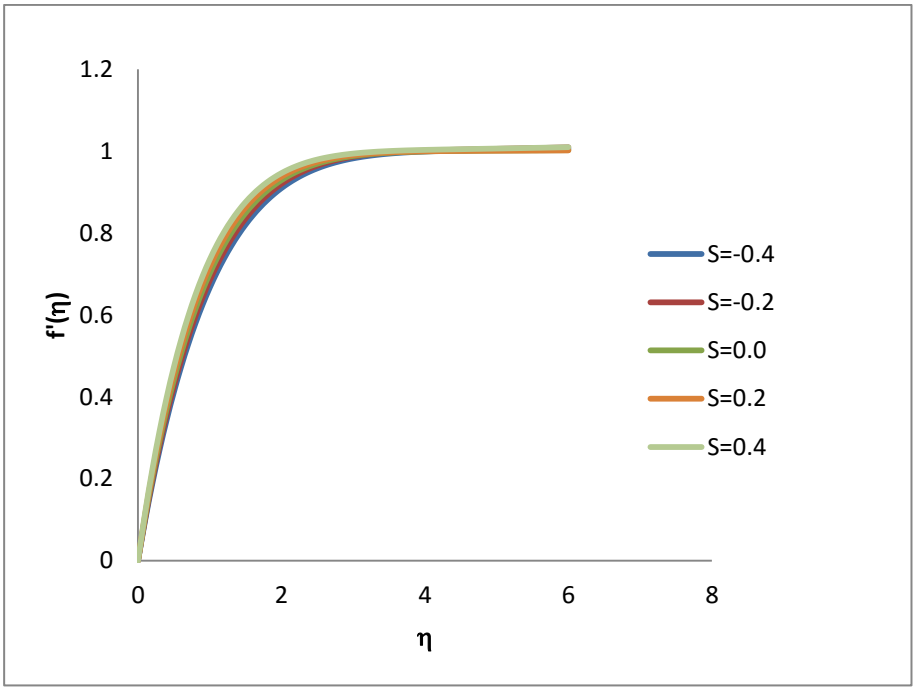

Fig 3.21 Velocity $f'(\eta)$ for various values of suction / blowing parameter S; Pr =7.0; Sc = 0.3; Sr = 0.3; k = 0.2; M = 1.0; $\delta = \beta = \varsigma = 0.0$*

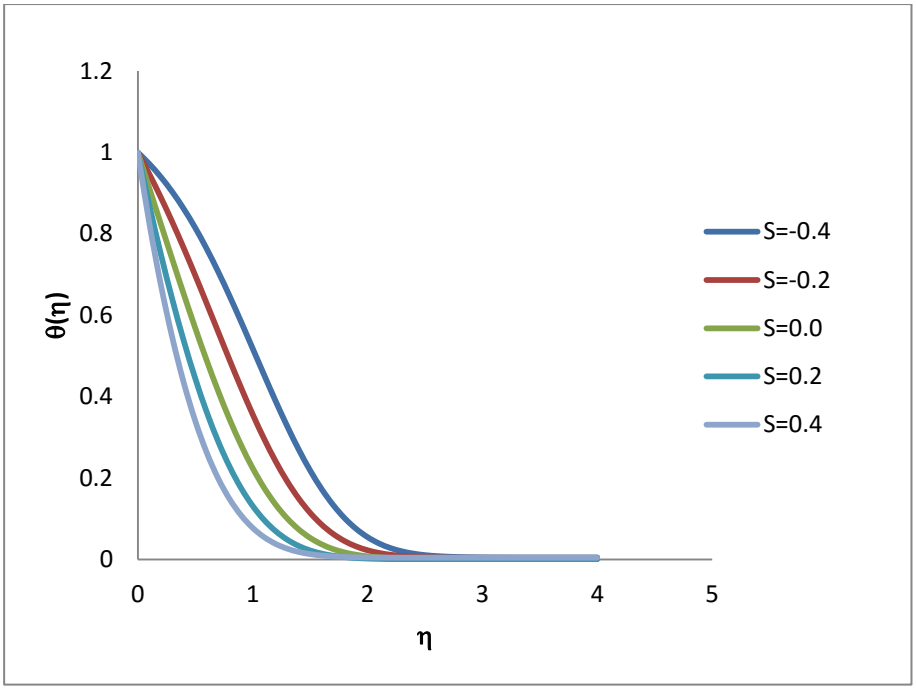

Fig 3.22 Temperature $\theta(\eta)$ for various values of suction/blowing parameter S; Pr = 7.0; Sc = 0.3; Sr = 0.3; k = 0.2; M = 1.0; $\delta = \beta = \varsigma = 0.0$*

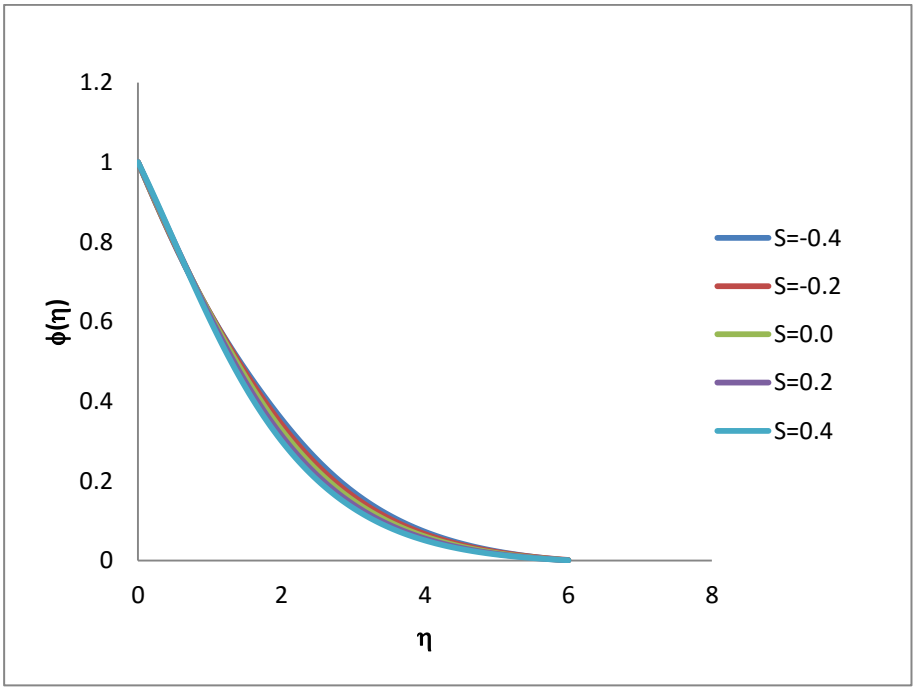

Fig 3.23 Concentration $\phi(\eta)$ for various values of suction/blowing parameter S; Pr = 7.0; Sc = 0.3; Sr = 0.3; k = 0.2; M = 1.0; $\delta = \beta = \varsigma = 0.0$*

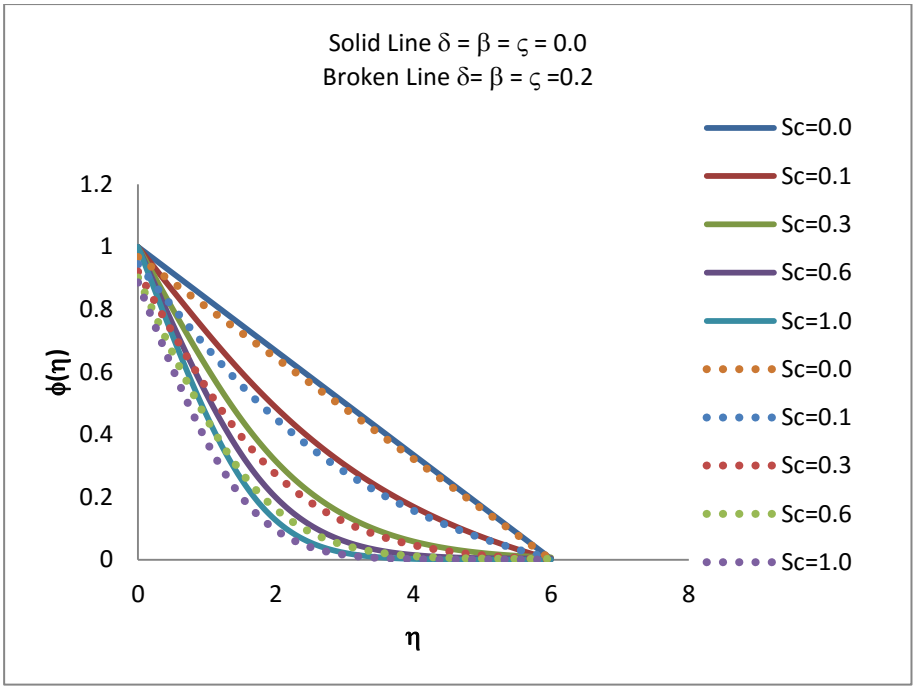

Fig 3.24 Concentration $\phi(\eta)$ for various values of Sc with the slip and no-slip boundary conditions; Pr =7.0; Sr=0.3; S= 0.2; k = 0.2; M = 1.0*

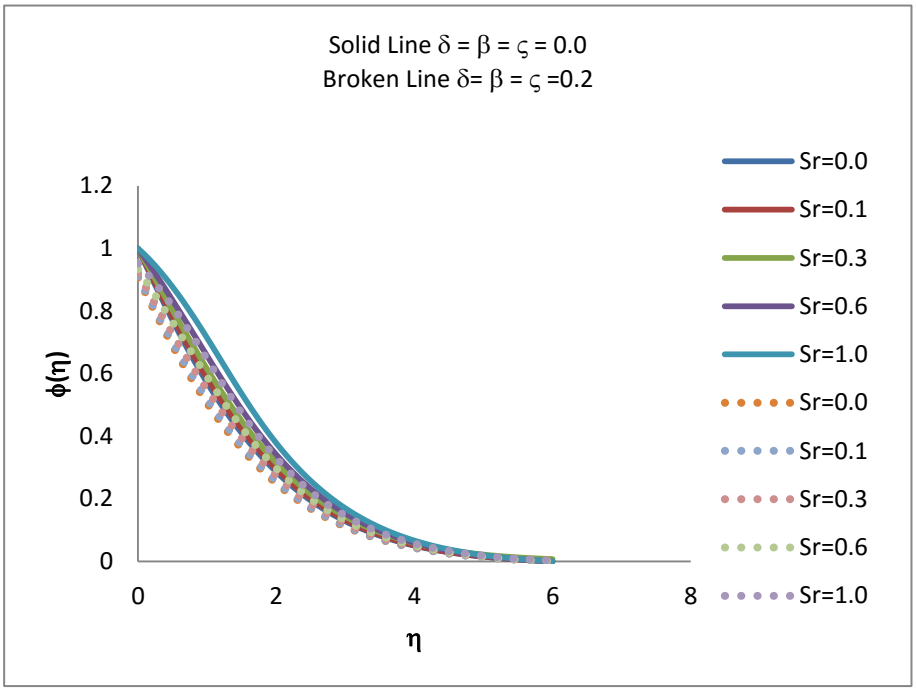

Fig 3.25 Concentration $\phi(\eta)$ for various values of Sr with the slip and no-slip boundary conditions; Pr=7.0; Sc= 0.3; S=0.2; k=0.2; M=1.0*

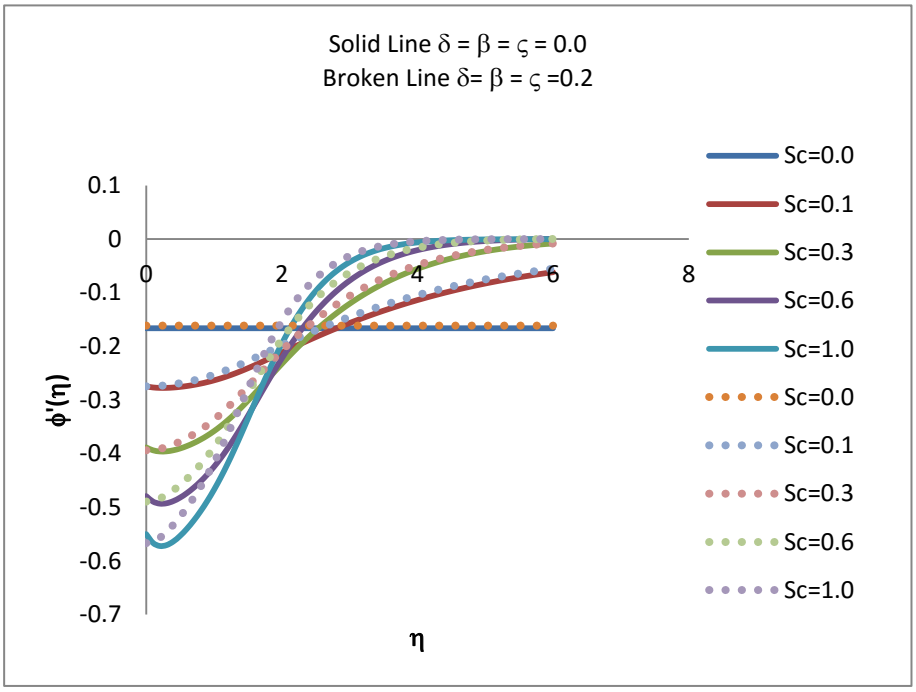

Fig 3.26 Rate of mass transfer $\phi'(\eta)$ for various values of Sc with the slip and no-slip boundary conditions; Pr =7.0; Sr=0.3; S= 0.2; k = 0.2; M=1.0*

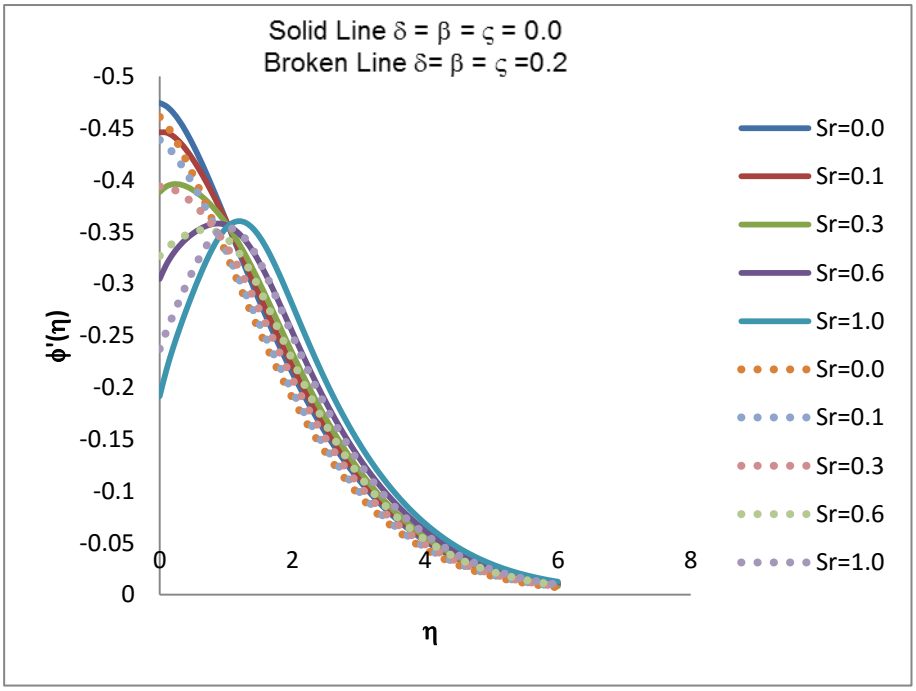

Fig 3.27 Rate of mass transfer $\phi'(\eta)$ for various values of Sr with the slip and no-slip boundary conditions; Pr =7.0; Sc = 0.3; S = 0.2;k= 0.2; M=1.0*

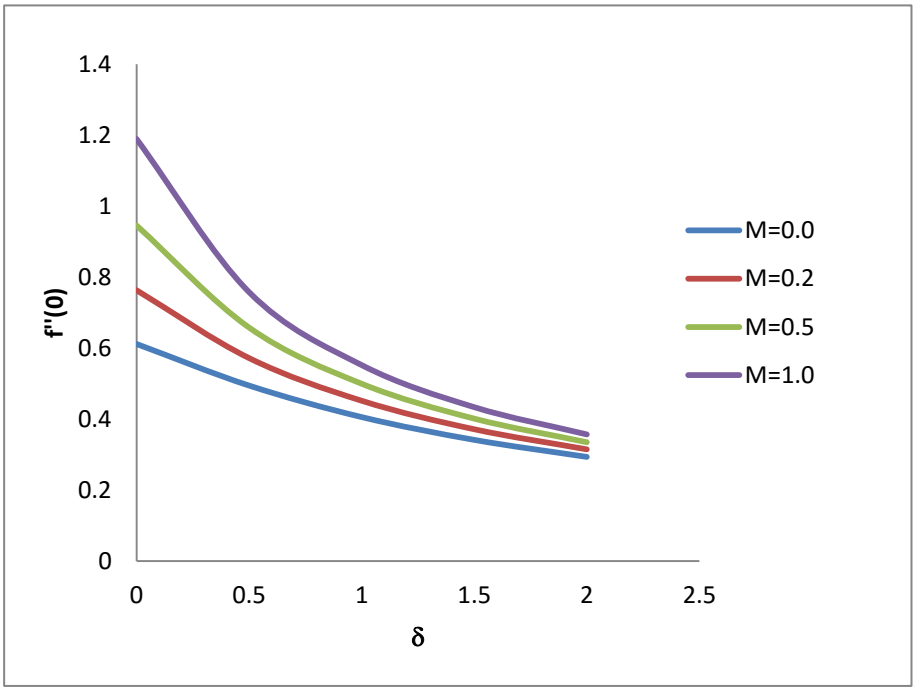

Fig 3.28 Skin-friction coefficient $f''(0)$ against δ for various values of M; Pr = 7.0; Sc = 0.3; Sr = 0.3; k = 0.2; S = 0.2; β = 0.2; ς = 0.2*

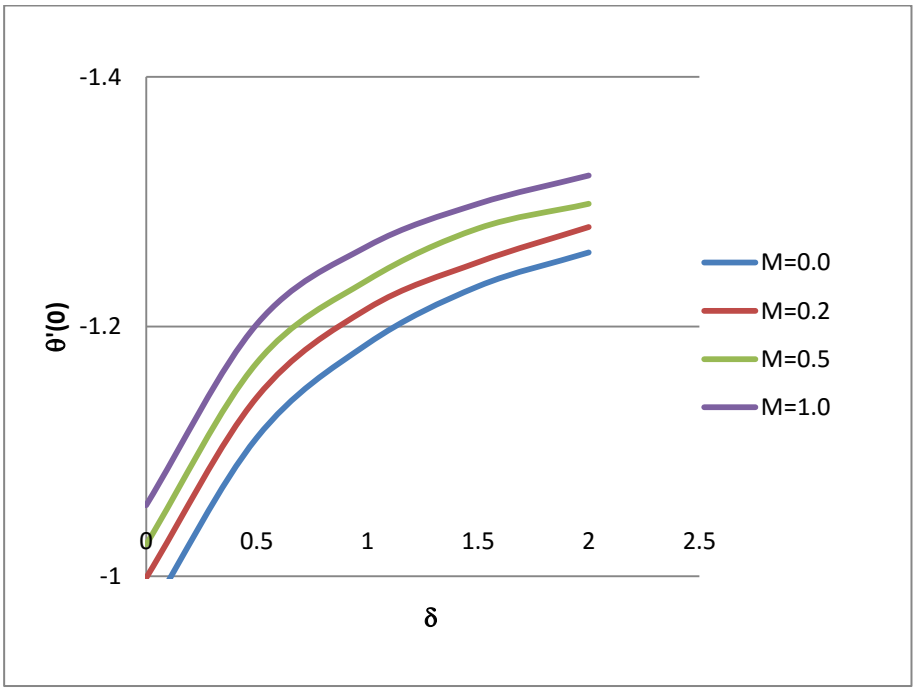

Fig 3.29 Rate of heat transfer $\theta'(0)$ against δ for various values of M; Pr = 7.0; Sc = 0.3; Sr = 0.3; k = 0.2; S = 0.2; β = 0.2; ς = 0.2*

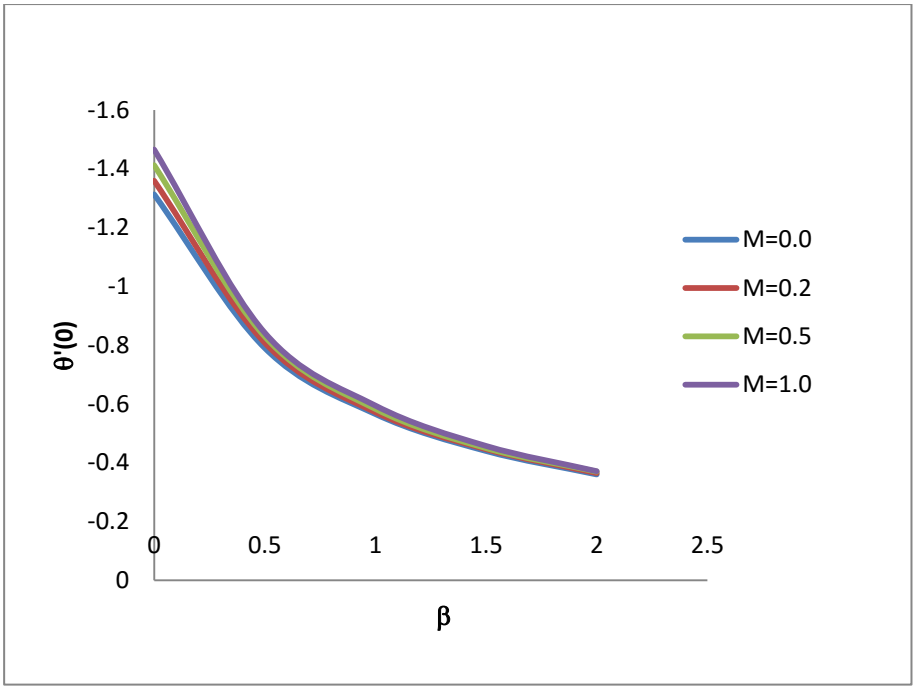

Fig 3.30 Rate of heat transfer $\theta'(0)$ against β for various values of M; Pr = 7.0; Sc = 0.3; Sr = 0.3; k = 0.2; S = 0.2; δ = 0.2; ς = 0.2*

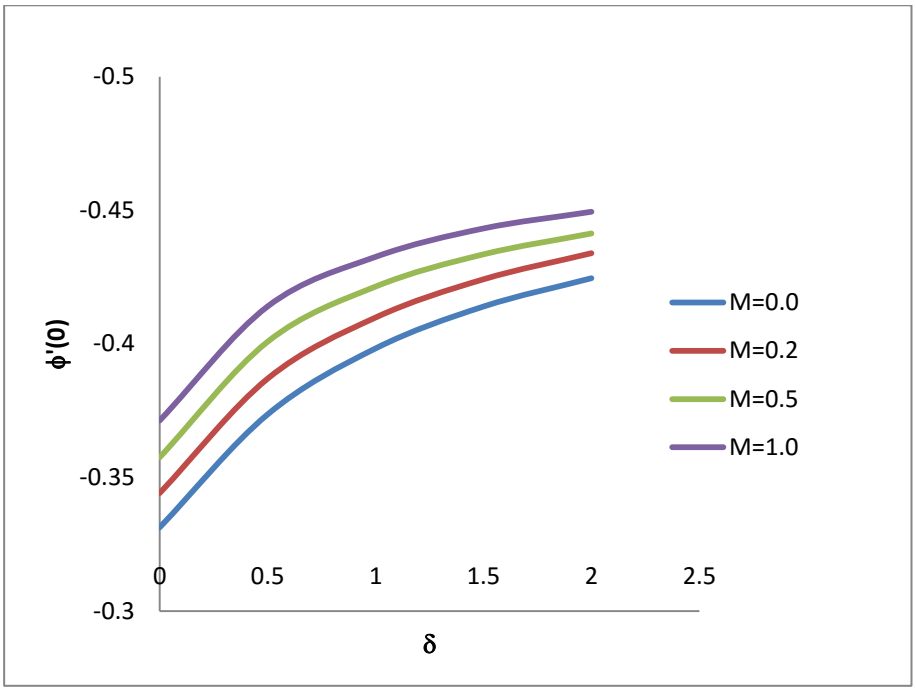

Fig 3.31 Rate of mass transfer $\phi'(0)$ against δ for various values of M; Pr = 7.0; Sc = 0.3; Sr = 0.3; k = 0.2; S = 0.2; β = 0.2; ς = 0.2*

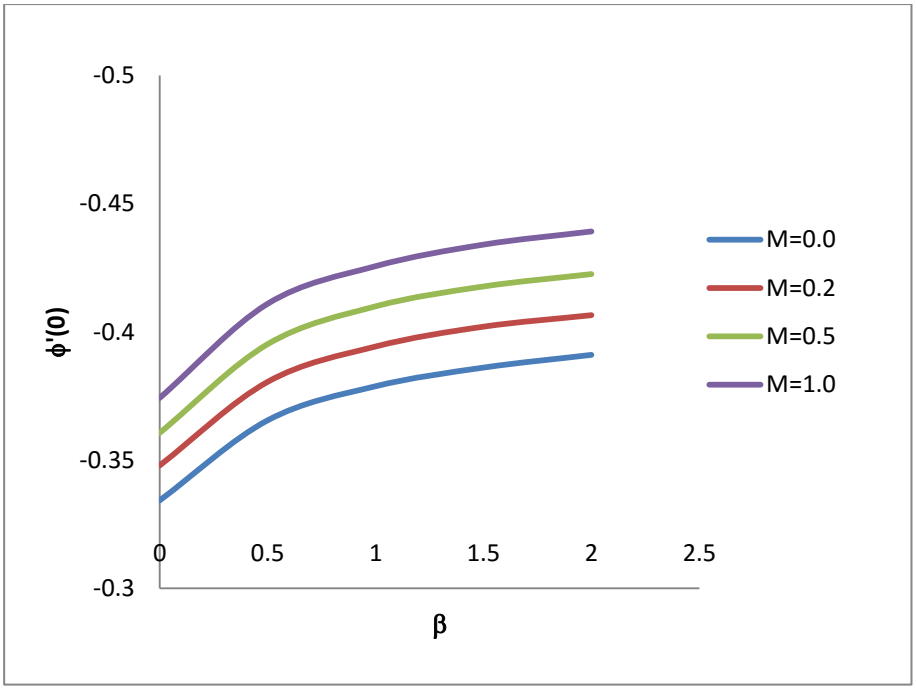

Fig 3.32 Rate of mass transfer $\phi'(0)$ against β for various values of M; Pr = 7.0; Sc = 0.3; Sr = 0.3; k = 0.2; S = 0.2; δ = 0.2; ς = 0.2*

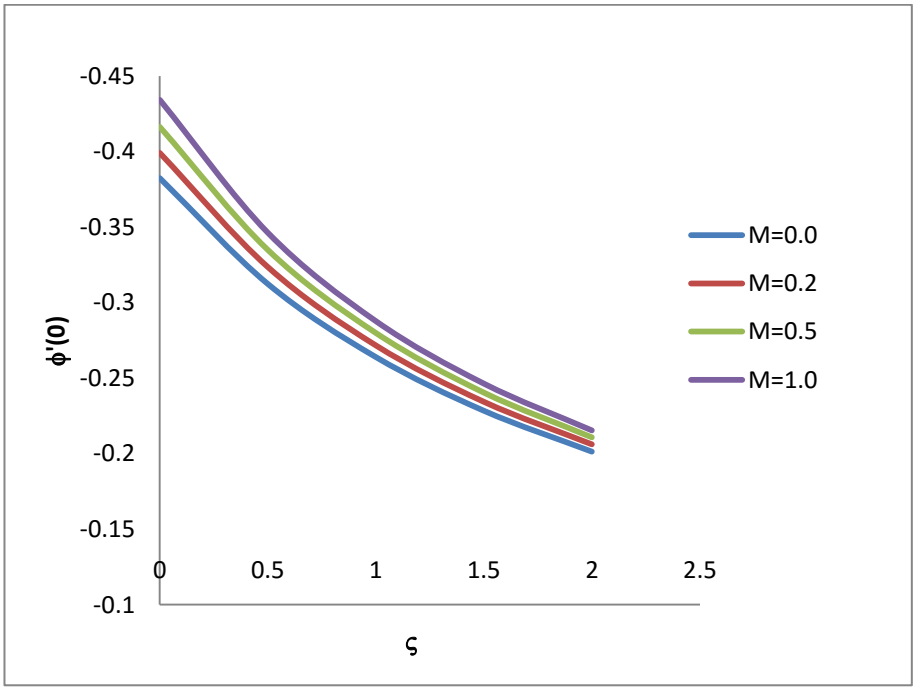

Fig 3.33 Rate of mass transfer $\phi'(0)$ against ς for various values of M; Pr = 7.0; Sc = 0.3; Sr = 0.3; k = 0.2; S = 0.2; δ = 0.2; β = 0.2*